## Supplementary Information

# Single-molecule fingerprinting of protein-drug interaction using a funneled biological nanopore

Ki-Baek Jeong[1,2,†], Minju Ryu[1,3,†], Jin-Sik Kim[1,2,†], Minsoo Kim[4], Jejoong Yoo[4], Minji Chung[1], Sohee Oh[1], Gyunghee Jo[5], Seong-Gyu Lee[5], Ho Min Kim[5,6], Mi-Kyung Lee[1,2,3,*], Seung-Wook Chi[1,3,7,*]

[1]Disease Target Structure Research Center, Division of Biomedical Research, Korea Research Institute of Bioscience and Biotechnology (KRIBB), Daejeon 34141, Republic of Korea

[2]Critical Diseases Diagnostics Convergence Research Center, KRIBB, Daejeon 34141, Republic of Korea

[3]Department of Proteome Structural Biology, KRIBB School of Bioscience, University of Science and Technology, Daejeon 34113, Republic of Korea

[4]Department of Physics, Sungkyunkwan University, Suwon, Gyeonggi 16419, Republic of Korea

[5]Center for Biomolecular and Cellular Structure, Institute for Basic Science (IBS), Daejeon 34126, Republic of Korea

[6]Graduate School of Medical Science and Engineering, Korea Advanced Institute of Science and Technology (KAIST), Daejeon 34141, Republic of Korea

[7]School of Pharmacy, Sungkyunkwan University, Suwon, Gyeonggi 16419, Republic of Korea

Corresponding authors: miki@kribb.re.kr, swchi@kribb.re.kr

† These authors contributed equally.

**Contents**

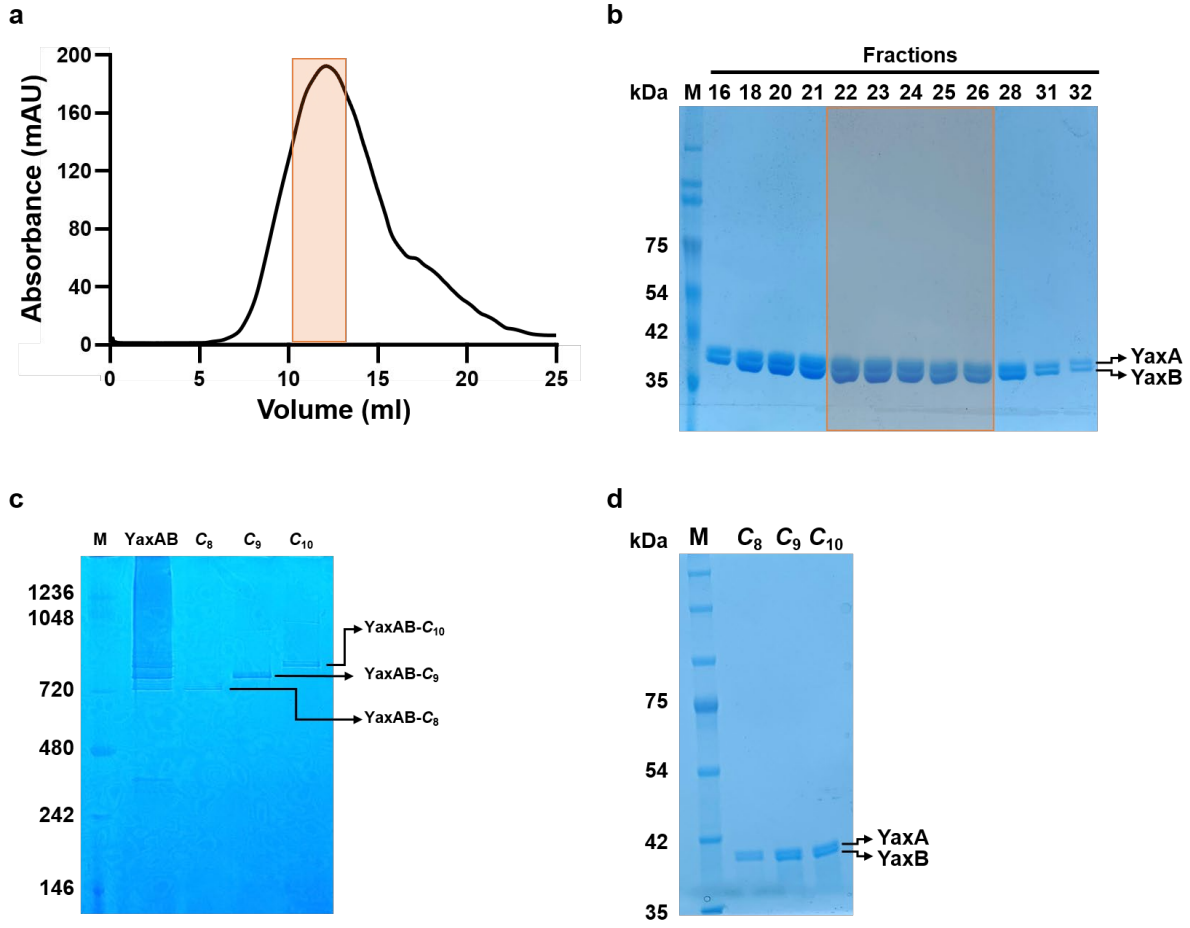


**Supplementary Fig. 1: Purification of YaxAB pores. a-d.** The chromatogram of size exclusion chromatography using the Superose 6 column (**a**) and SDS-PAGE gel image of purified YaxAB complex (**b**). (**c**) The native gel image of three YaxAB oligomeric states, YaxAB-$C_8$ (16-mer), YaxAB-$C_9$ (18-mer), and YaxAB-$C_{10}$ (20-mer), separated via gel extraction. (**d**) The SDS-PAGE gel image of the three YaxAB oligomeric states (YaxAB-$C_8$, YaxAB-$C_9$, and YaxAB-$C_{10}$) extracted from gel. All gel images include a size marker (lane M). The representative PAGE result is shown (n = 3 independent replicates). Source data are provided as a Source Data file.

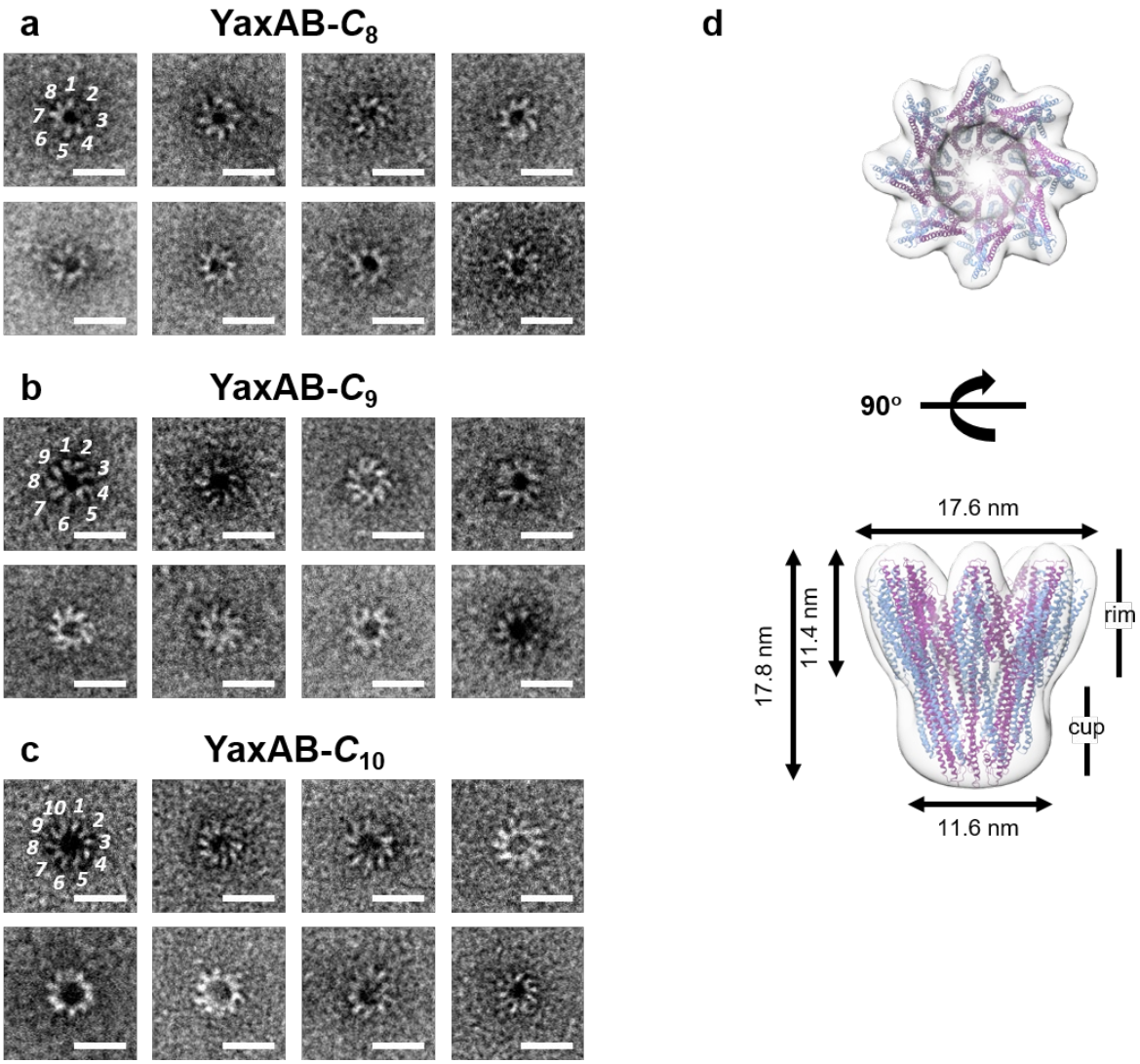


**Supplementary Fig. 2: Negative-staining electron microscopy (EM) image of YaxAB pore and the structure of YaxAB-$C_8$. a-c.** Top view of YaxAB-$C_8$ (**a**), YaxAB-$C_9$ (**b**), and YaxAB-$C_{10}$ (**c**) pores cropped from raw micrographs of EM. The representative microscopy image is presented (n = 2 independent replicates). Source data are provided as a Source Data file. **d.** 3D volume and structural model of YaxAB-$C_8$ highlighting views along the $C_8$ symmetry axis and side views of the YaxAB-$C_8$ pore. YaxA and YaxB are colored blue and purple, respectively. Scale bar = 25 nm.

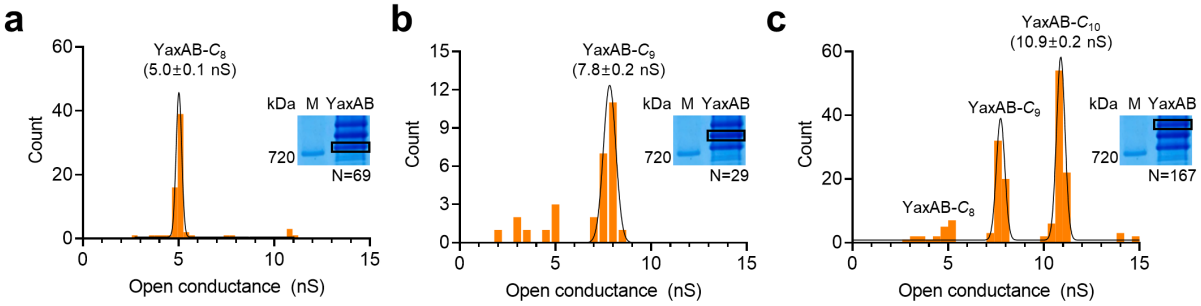


**Supplementary Fig. 3: Open conductance distributions of YaxAB nanopores. a-c**. Three types of YaxAB pore protein were collected from three separate bands on the blue native gel (4-16 %). Each conductance histogram was derived from nanopore experiments using YaxAB-$C_8$ (**a**), YaxAB-$C_9$ (**b**), or YaxAB-$C_{10}$ (**c**) (black box). Conductance of each pore was recorded at 100 mV (*cis* side) in 1 M KCl at pH 7.5. In total, 265 nanopores were tested for pore insertion. All gel images include a size marker (lane M).

**a**

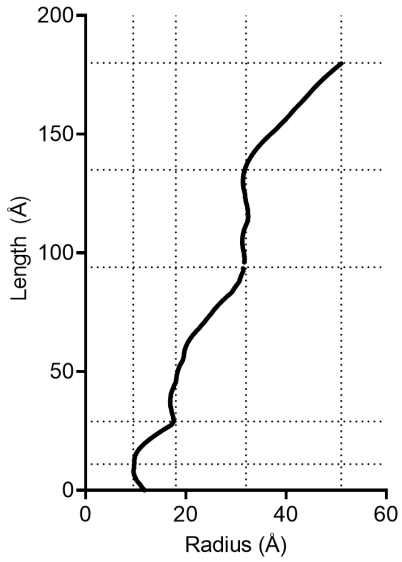


**b**

| | Experimental (pA) | Theoretical (pA) |
|---|---|---|
| YaxAB-$C_8$ | 506.06 ± 6.35 | 542.58 |
| YaxAB-$C_9$ | 776.04 ± 17.37 | 823.46 |
| YaxAB-$C_{10}$ | 1086.52 ± 16.50 | 1173.88 |

**Supplementary Fig. 4: Electrophysiological characterization of YaxAB nanopores. a.** Radius and length of the YaxAB-$C_8$ nanopore were estimated using the program HOLE. **b.** Comparison between experimental and theoretical ionic currents of each pore. At an applied voltage of 100 mV, experimental and theoretical ionic currents were well-matched. The theoretical ionic currents were calculated from the inverse of the total resistance ($R_{pore}$) for funnel geometry of each pore, derived from YaxAB models (Equation 3, Methods section).

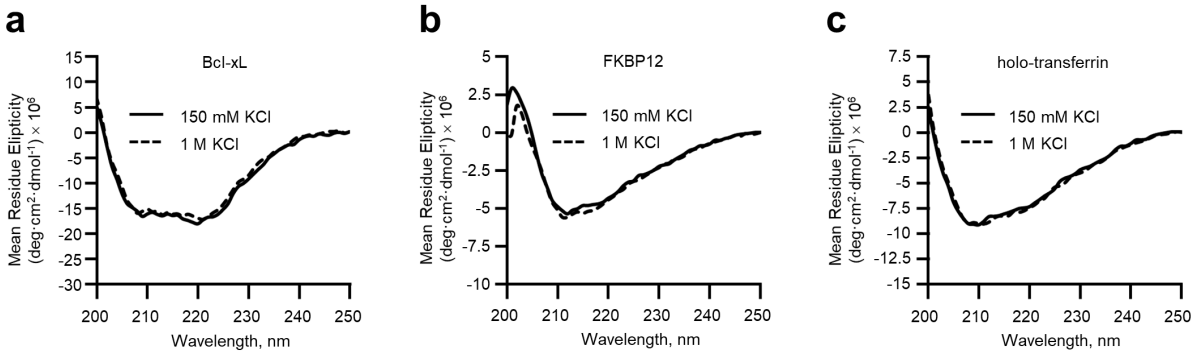


**Supplementary Fig. 5. The circular dichroism (CD) analysis of protein analytes. a-c**. The CD spectra of Bcl-xL (**a**), FKBP12 (**b**), and holo-transferrin (**c**) in the nanopore measurement buffer containing 150 mM and 1 M KCl.

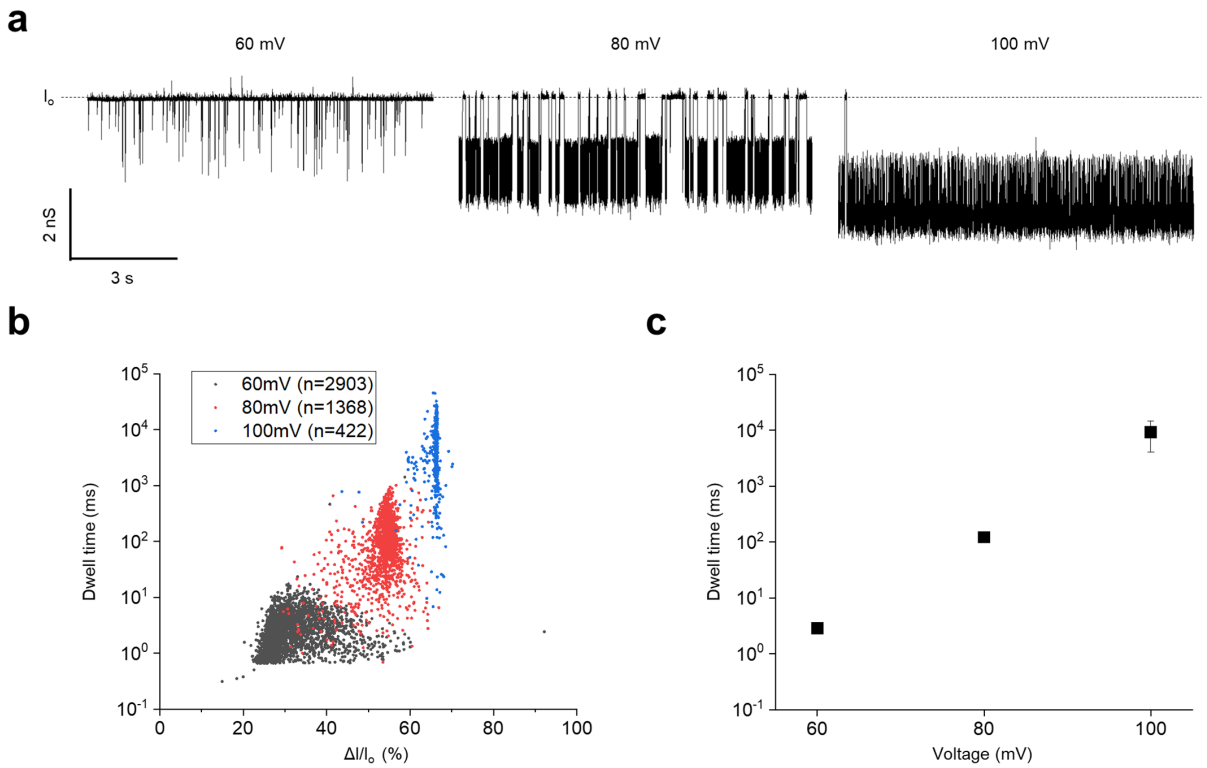


**Supplementary Fig. 6: Measurement of dwell times of Bcl-xL using YaxAB nanopores at different voltages. a.** Representative current traces of Bcl-xL at various applied voltages (60, 80, and 100 mV). **b.** The scatter plot of dwell time *vs.* relative current blockades ($\Delta I/I_o$) of nanopore events obtained at 60 mV (black), 80 mV (red), and 100 mV (blue). **c.** The voltage-dependence on dwell times of nanopore events obtained from Bcl-xL. The mean values of dwell times at 60, 80 and 100 mV are 2.85 ± 0.30 ms, 120.93 ± 12.45 ms, and 9292.96 ± 5200.98 ms, respectively. Data are presented as mean ± SD, n = 3 independent replicates for each engaged voltage. Source data are provided as a Source Data file.

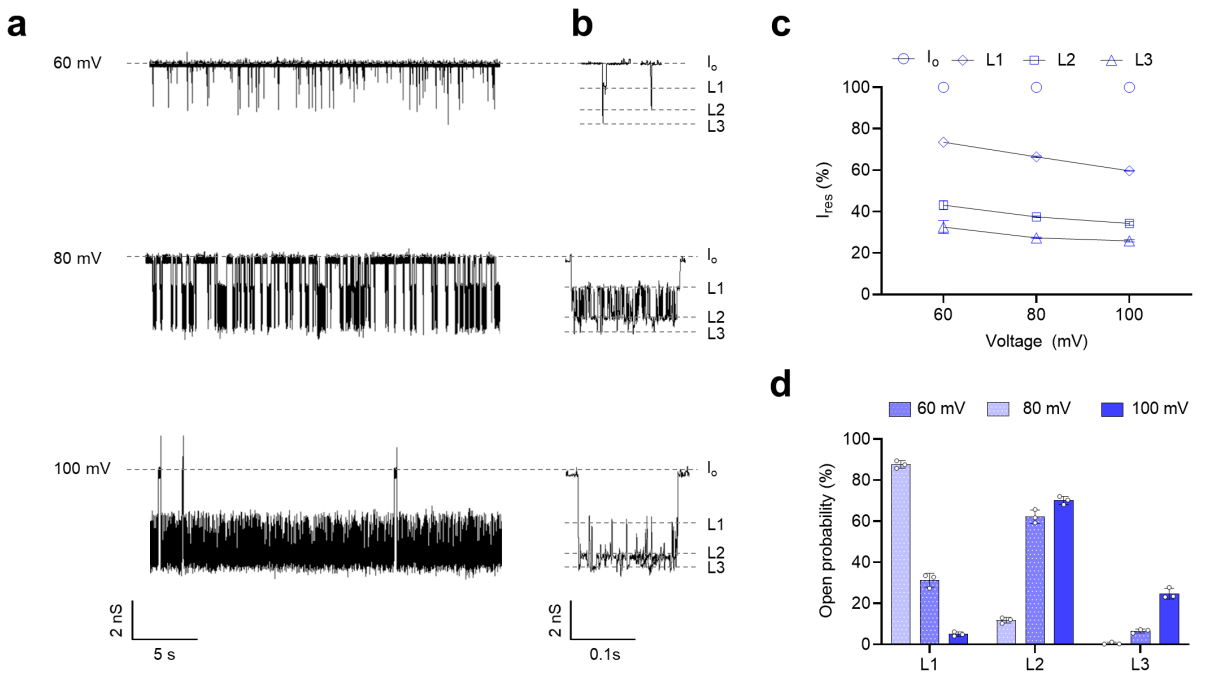


**Supplementary Fig. 7: Current blockade analysis of Bcl-xL using YaxAB nanopores at different voltages. a.** Representative current traces of Bcl-xL trapped by a YaxAB nanopore with engaged voltages (60, 80, and 100 mV) and a 1 kHz filter. $I_o$ indicates open current of the nanopore, and each ionic current levels are L1, L2, and L3, respectively. Residual current ($I_{res}$) gradually decreased with voltage increase until 100 mV. **b.** Representative nanopore events exhibiting vibration signals. **c.** Residual current of Bcl-xL trapped by YaxAB nanopore decreased with voltage increment (60 to 100 mV). Data are presented as mean ± SD, n = 3 independent replicates for voltages (60, 80, and 100 mV). The ratio of residual current of L1 to L3 levels at different voltage biases; L1 (73.54 ± 1.08%), L2 (43.14 ± 2.19%), and L3 (32.54 ± 3.14%) at 60 mV; L1 (66.43 ± 0.36%), L2 (37.44 ± 0.42%), and L3 (27.33 ± 0.28%) at 80 mV; L1 (59.72 ± 0.17%), L2 (34.26 ± 0.87%), and L3 (25.85 ± 0.52%) at 100 mV. Source data are provided as a Source Data file. **d.** Open probability of each peak level in Bcl-xL as a function of engaged voltages. Data are presented as mean ± SD, n = 3 independent replicates for each engaged voltage. The open probability of L1 to L3 current levels at different voltage biases: L1 (87.62 ± 1.82%), L2 (11.82 ± 1.37%), and L3 (0.57 ± 0.54%) at 60 mV; L1 (31.25 ± 3.38%), L2 (62.18 ± 3.29%), and L3 (6.58 ± 0.92%) at 80 mV; L1 (5.04 ± 1.05%), L2 (70.19 ± 1.95%), and L3 (24.76 ± 2.6%) at 100 mV. Source data are provided as a Source Data file.

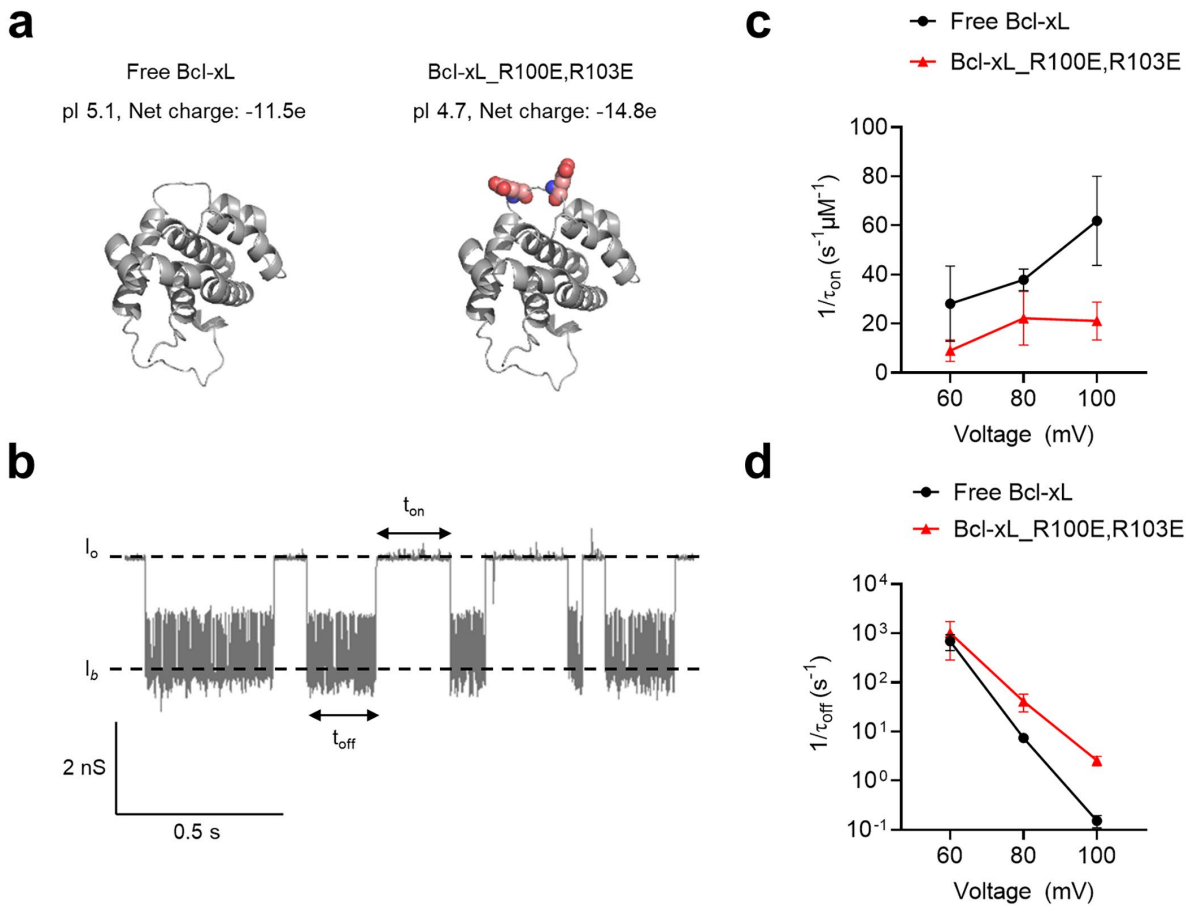


**Supplementary Fig. 8: The capture rate and trapping event frequency of wild-type and mutant Bcl-xL measured by YaxAB nanopores at different voltages. a.** Net-charge properties of wild-type and mutant Bcl-xL (Bcl-xL_R100E,R103E)**.** The mutation sites are indicated as spheres (red and blue) in Bcl-xL structure (gray). **b.** The representative current trace of wild-type Bcl-xL at 80 mV with the definition of event parameter. The interevent interval ($t_{on}$) and the dwell time ($t_{off}$) are defined as marked on the current trace. The mean time constants ($\tau_{on}$ and $\tau_{off}$) were derived by fitting exponential decay with histograms of $t_{on}$ and $t_{off}$ at the various applied voltage (60, 80, and 100 mV), respectively. **c.** Plots of capture rate ($1/\tau_{on}$) *vs.* applied voltage of wild-type Bcl-xL (black circle) and mutant Bcl-xL (red triangle). Data are presented as mean ± SD, n = 3 independent replicates for wild-type Bcl-xL at 60 and 80 mV, n = 2 independent replicates for wild-type at 100 mV. The value of $1/\tau_{on}$: free Bcl-xL, 28.14 ± 15.31, 37.85 ± 4.38, 61.84 ± 18.16 $s^{-1}\mu M^{-1}$; the mutant Bcl-xL, 9.01 ± 4.40, 22.19 ± 10.92, 21.10 ± 7.70 $s^{-1}\mu M^{-1}$ at different voltage biases (60, 80, and 100 mV). Source data are provided as a Source Data file. **d.** Plots of $1/\tau_{off}$ *vs.* applied voltage. Data are presented as mean ± SD, n = 3 independent replicates. The value of $1/\tau_{off}$: free Bcl-xL, 691.47 ± 248.61, 7.38 ± 0.85, 0.15 ± 0.04 $s^{-1}$; the mutant Bcl-xL, 1013.97 ± 729.04, 41.15 ± 16.27, 2.57 ± 0.56 $s^{-1}$ at different voltage biases (60, 80, and 100 mV). Source data are provided as a Source Data file.

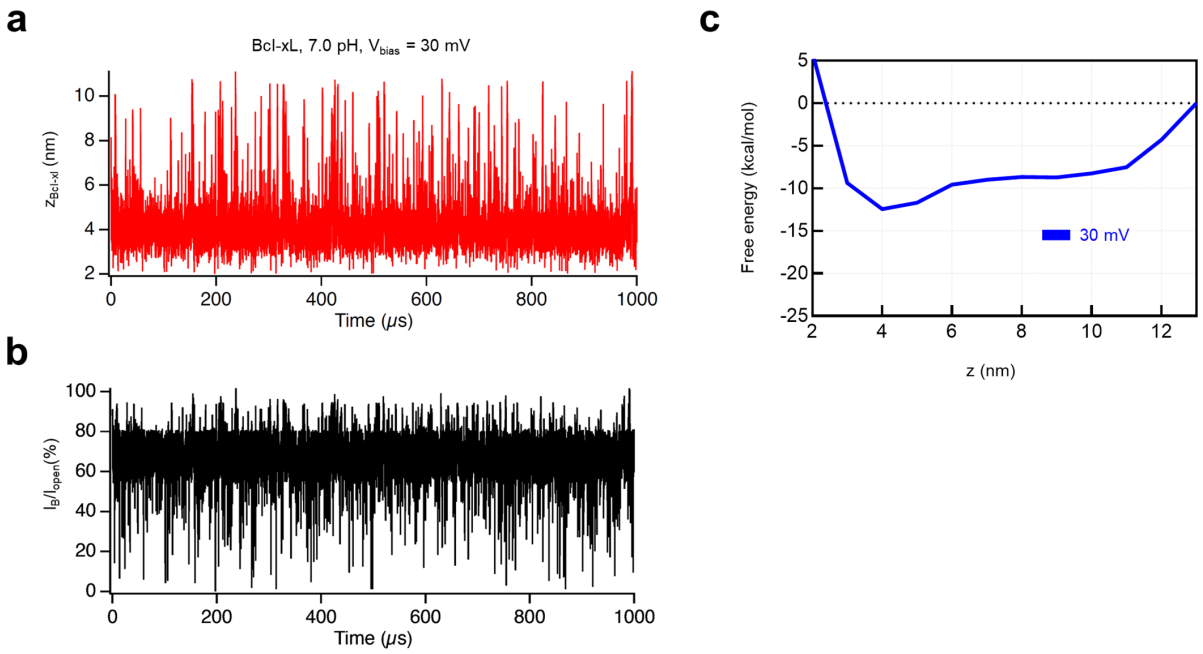


**Supplementary Fig. 9: The Brownian dynamics simulation used to model Bcl-xL movement within a YaxAB nanopore.** The position (**a**) and relative current blockade (**b**) of Bcl-xL were calculated by Brownian dynamics simulations performed at pH 7.0 at 30 mV. The condition was optimized to prove the presence of two levels of Bcl-xL in a YaxAB nanopore. (**c**) Free energy landscapes of Bcl-xL within a YaxAB nanopore at 30 mV.

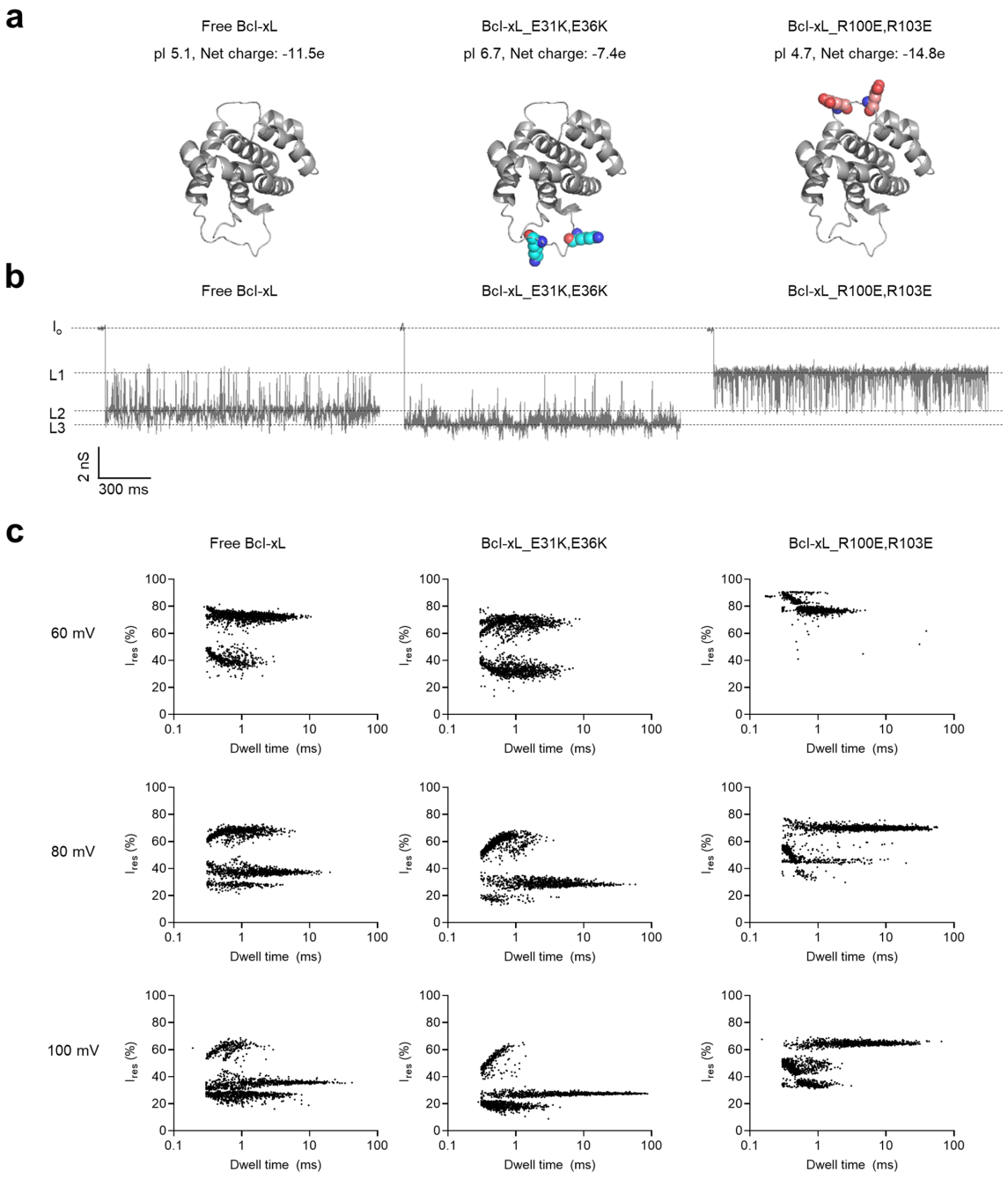


**Supplementary Fig. 10: Distinctive current signal patterns of Bcl-xL and its mutants measured by YaxAB nanopores at different voltages. a.** Bcl-xL and its variants (Bcl-xL_E31K,E36K as a positively charged mutant and Bcl-xL_R100E,R103E as a negatively charged mutant). The mutation sites are indicated as spheres (red and blue) in Bcl-xL structure (gray). **b.** Representative multi-level current blockades for each analyte measured at 100 mV. **c.** The scatter plot ($I_{res}$ versus. dwell time) for wild-type Bcl-xL and its variants at various voltages (60, 80, and 100 mV). All electrical current was filtered with a low-pass Bessel filter at 1 kHz with a sampling rate of 100 kHz. All of statistical analysis was performed over 2,000 events.

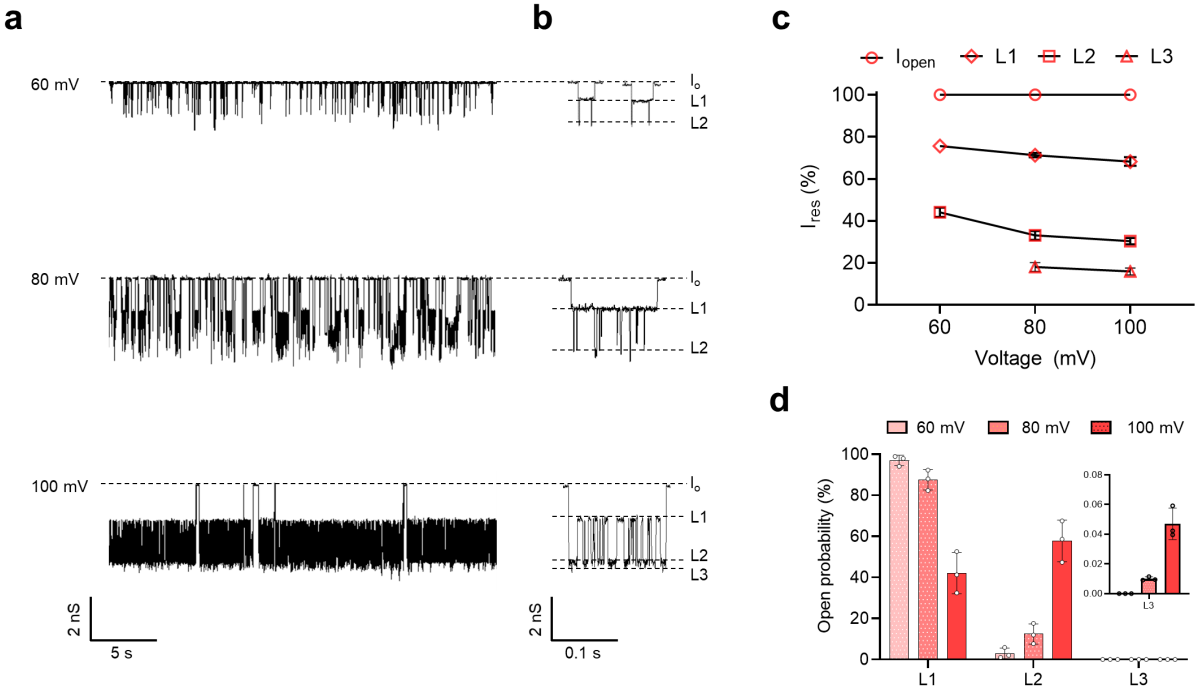


**Supplementary Fig. 11: Current blockades analysis of Bcl-xL/Bak-BH3 complex using YaxAB nanopores at different voltages. a.** Representative current traces of the Bcl-xL/Bak-BH3 complex trapped by a YaxAB nanopore with engaged voltages (60, 80, and 100 mV) and a 1 kHz filter. $I_o$ indicates open current of the nanopore, and each ionic current levels are L1, L2, and L3, respectively. Residual current ($I_{res}$) gradually decreased with voltage increase until 100 mV. **b.** Representative nanopore events exhibiting vibration signals. **c.** Residual current of Bcl-xL/Bak-BH3 trapped by the YaxAB nanopore decreased with voltage increment (60 to 100 mV). Data are presented as mean ± SD, n = 3 independent replicates at each engaged voltage. The ratio of residual current of L1 to L3 levels at different voltage biases; L1 (75.67 ± 0.17%) and L2 (44.04 ± 2.21%) at 60 mV; L1 (71.28 ± 1.02%), L2 (33.10 ± 2.06%), and L3 (18.06 ± 2.11%) at 80 mV; L1 (68.24 ± 2.06%), L2 (30.32 ± 1.50%), and L3 (15.91 ± 1.63%) at 100 mV. Source data are provided as a Source Data file. **d.** Open probability of each peak level in Bcl-xL/Bak-BH3 as a function of engaged voltages. Data are presented as mean ± SD, n = 3 independent replicates at each engaged voltage. The open probability of L1 to L3 current levels at different voltage biases: L1 (96.99 ± 2.54%) and L2 (3.01 ± 2.54%) at 60 mV; L1 (87.56 ± 4.97%), L2 (12.43 ± 4.97%), and L3 (0.01 ± 0.001%) at 80 mV; L1 (42.36 ± 10.09%), L2 (57.59 ± 10.09%), and L3 (0.05 ± 0.01%) at 100 mV. Magnified open probability of L3 at three different voltages (inset). Source data are provided as a Source Data file.

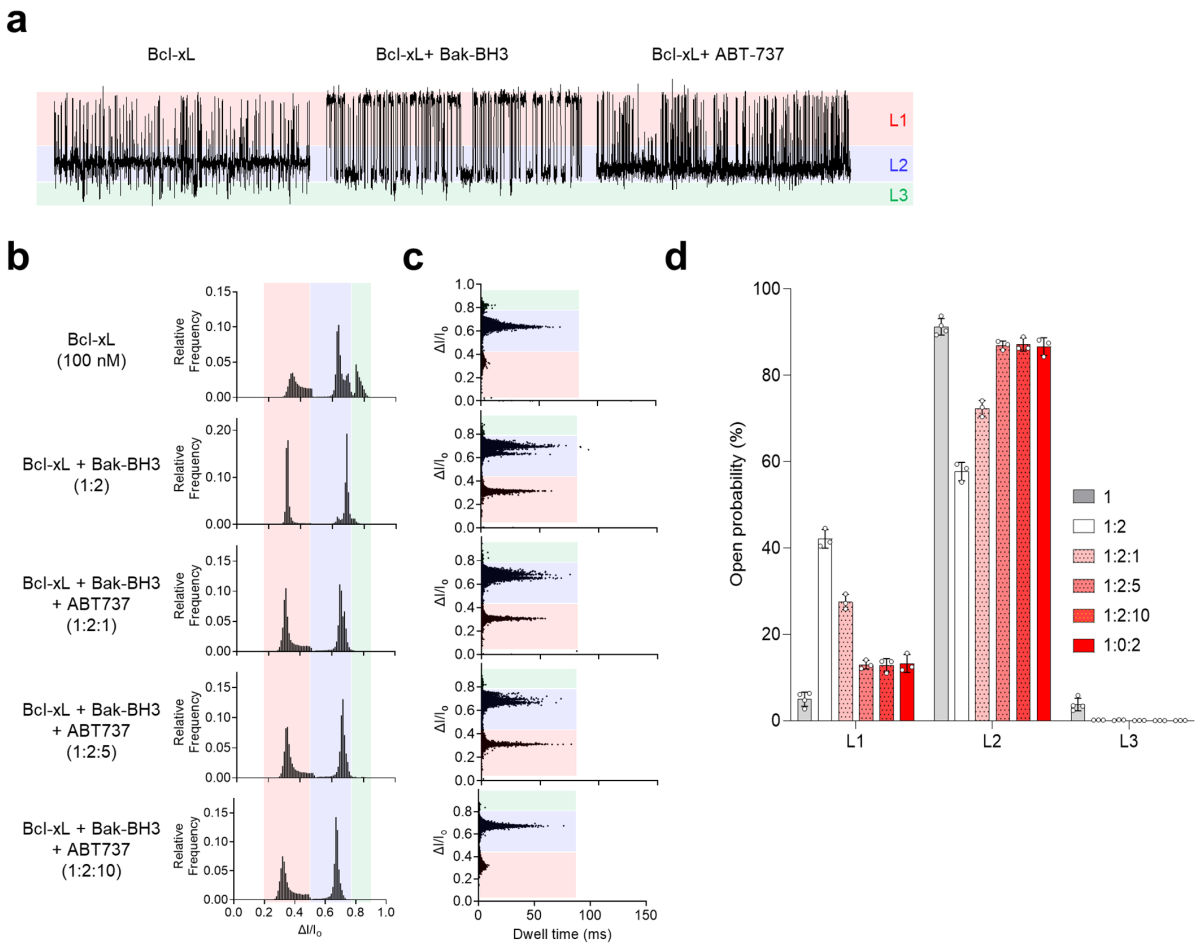


**Supplementary Fig. 12: Current blockade-based analysis of Bcl-xL/Bak-BH3 interaction inhibition by ABT-737 using YaxAB nanopores. a**. Representative current traces from Bcl-xL, Bcl-xL/Bak-BH3 complex (at the molar ratio of 1:2), and Bcl-xL/Bak-BH3 complex in the presence of ABT-737 (at the molar ratio of 1:2:10 Bcl-xL:Bak-BH3:ABT-737). All current blockades were categorized by three current levels (L1, L2, and L3). **b**. Statistical histograms of open probability of L1 to L3 current levels. The Bcl-xL/Bak-BH3 complex was titrated with ABT-737 at the molar ratios of 1:2:1, 1:2:5, and 1:2:10 to monitor the protein-protein interaction (PPI) inhibition by ABT-737. **c**. Scatter plots ($\Delta I/I_o$ vs. dwell time) of multi-level current blockades. All current traces were filtered using a Bessel (8-pole) 1 kHz filter. **d**. The Bcl-xL/Bak-BH3 (1:2) complex was titrated with ABT-737 at the molar ratios of 1:2:1, 1:2:5, and 1:2:10. Open probability of the Bcl-xL/ABT-737 (1:0:2) complex without Bak-BH3 was included for comparison. Data are presented as mean ± SD, n = 4 independent replicates for Bcl-xL; n = 3 independent replicates for the Bcl-xL/Bak-BH3 complex; n = 3 for Bcl-xL/Bak-BH3 complex in the presence of ABT-737. Source data are provided as a Source Data file. All electrical recordings were conducted in 1 M KCl at pH 7.5, with a 100 kHz sampling rate and a 10 kHz Bessel filter.

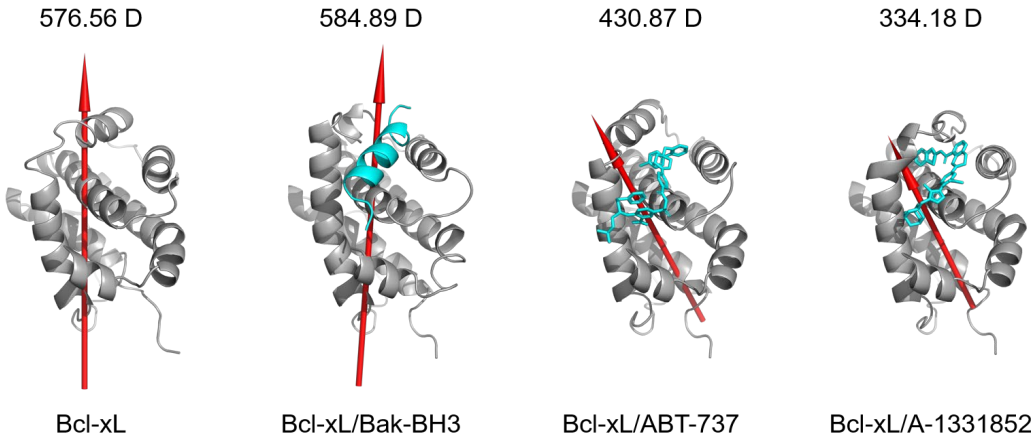


**Supplementary Fig. 13: Orientation and strength of dipole moment for free Bcl-xL and three Bcl-xL complexes (Bcl-xL/Bak-BH3, Bcl-xL/ABT-737, and Bcl-xL/A-1331852).** The dipole moments (Debye, D) were calculated by using a Discovery Studio software. The red arrows indicate the direction of the protein dipole. Bcl-xL and binders are shown in gray and cyan, respectively.

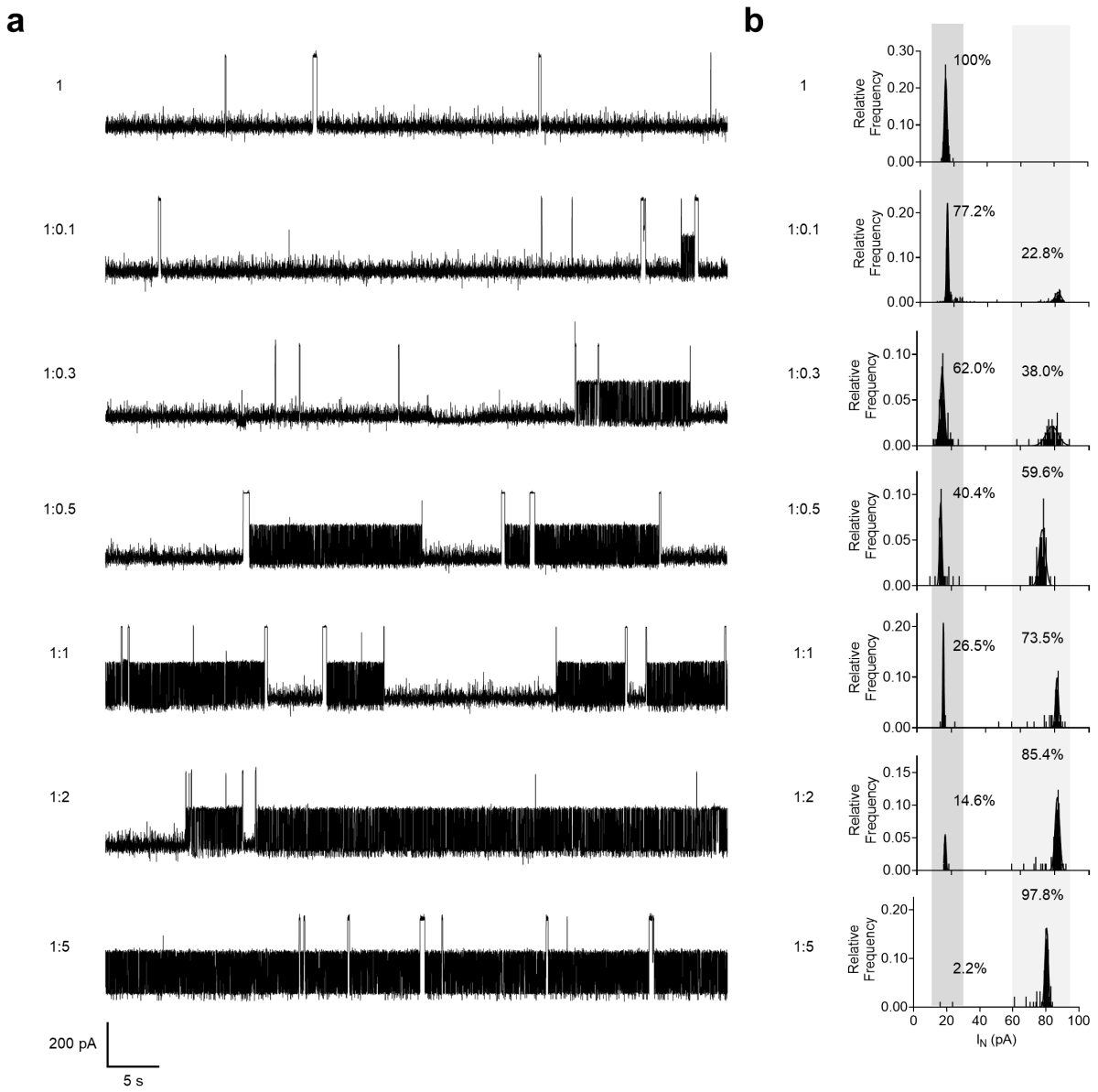


**Supplementary Fig. 14: Current noise ($I_N$)-based analysis of nanopore events upon titration of Bcl-xL with Bak-BH3. a**. Representative current traces obtained from titration of Bak-BH3 into Bcl-xL at the molar ratios of 1:0.1, 1:0.3, 1:0.5, 1:1, 1:2, and 1:5. **b**. Statistical histograms of $I_N$ values for each titration point**.**

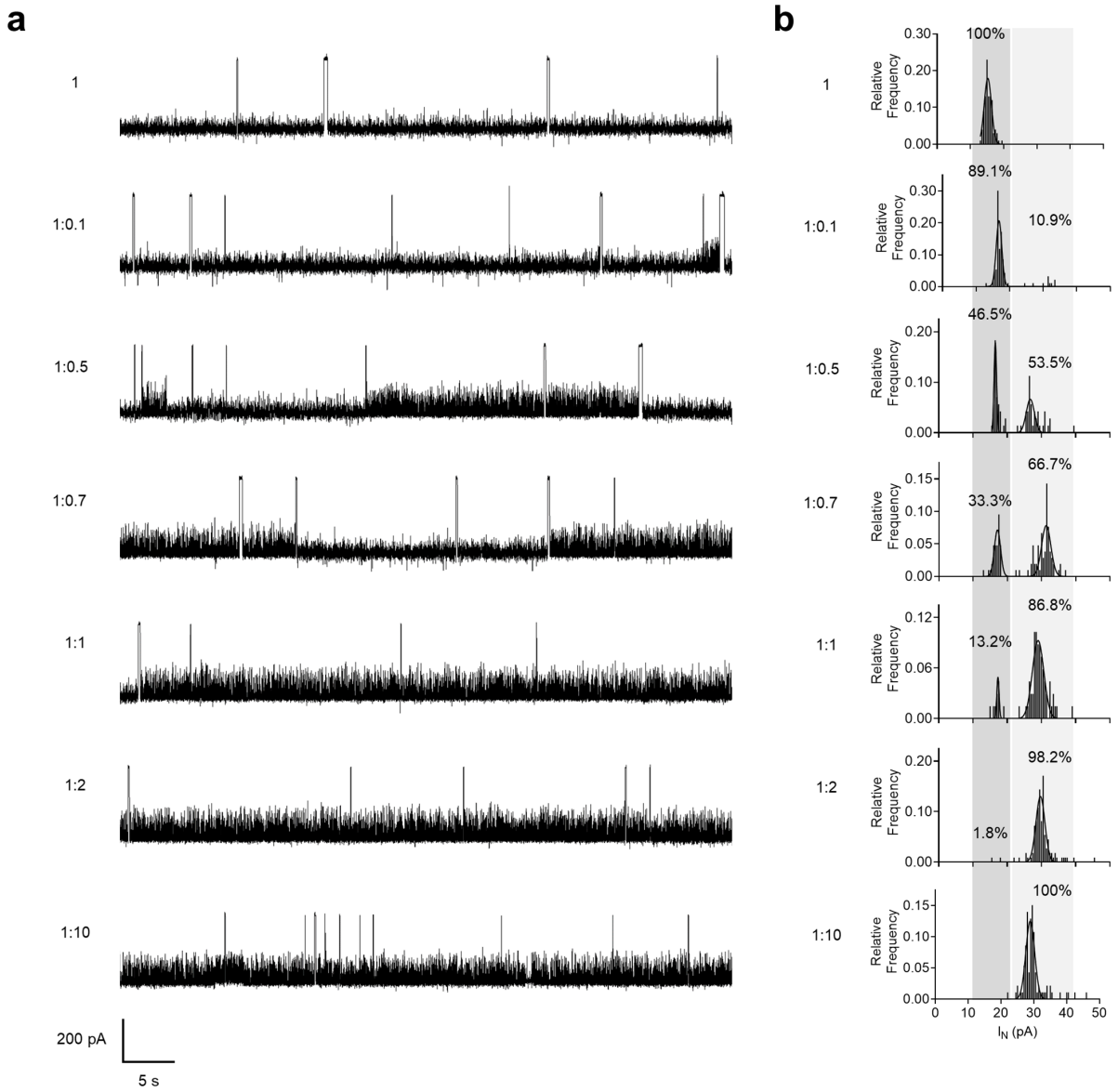


**Supplementary Fig. 15: Current noise ($I_N$)-based analysis of nanopore events upon titration of Bcl-xL with ABT-737. a**. Representative current traces obtained from titration of ABT-737 into Bcl-xL at the molar ratios of 1:0.1, 1:0.5, 1:0.7, 1:1, 1:2, and 1:10. **b**. Statistical histograms of $I_N$ values for each titration point**.**

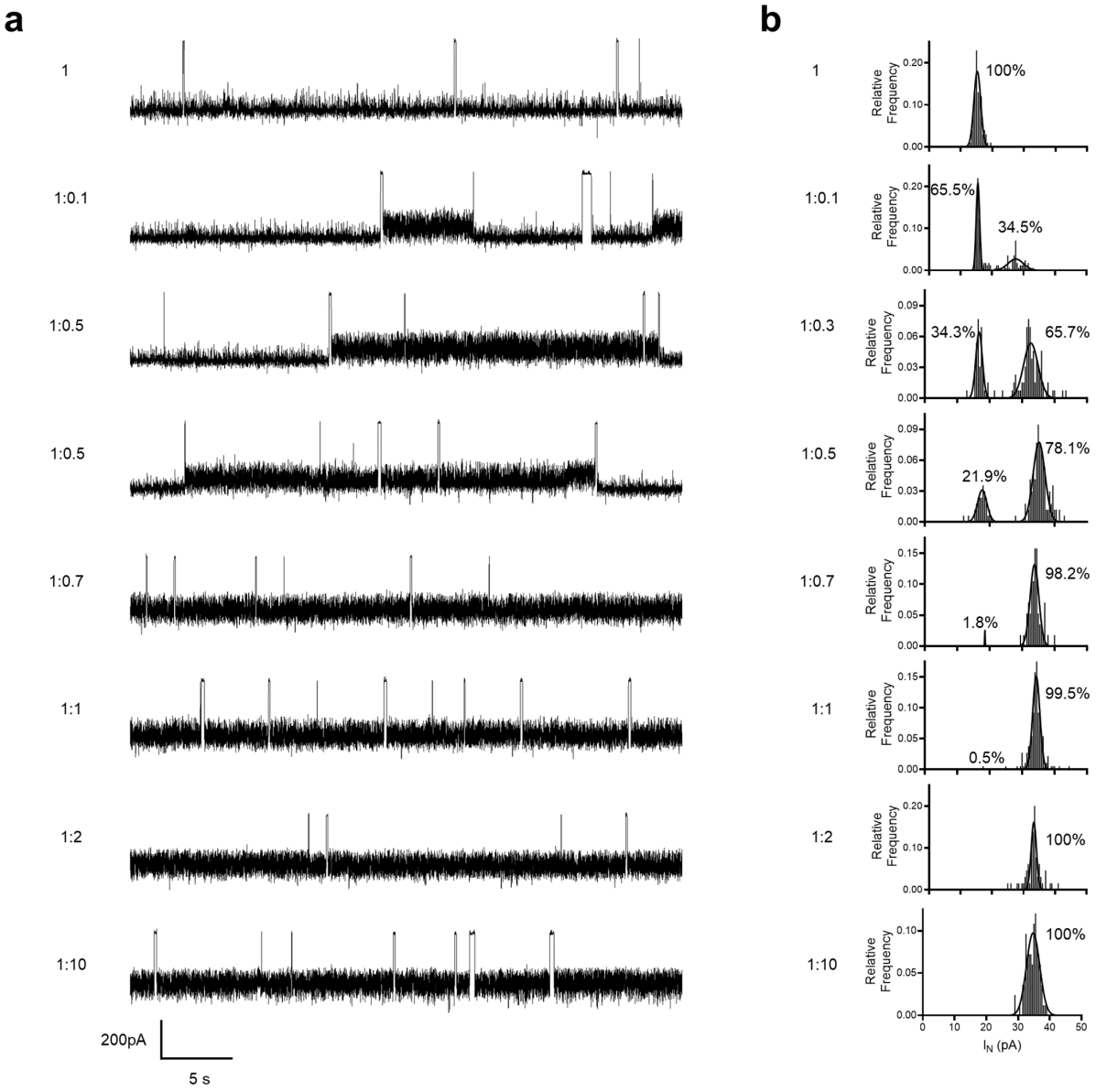


**Supplementary Fig. 16: Current noise ($I_N$)-based analysis of nanopore events upon titration of Bcl-xL with A-1331852. a**. Representative current traces obtained from titration of A-1331852 into Bcl-xL at the molar ratios of 1:0.1, 1:0.3, 1:0.5, 1:0.7, 1:1, 1:2, and 1:10. **b**. Statistical histograms of $I_N$ values for each titration point**.**

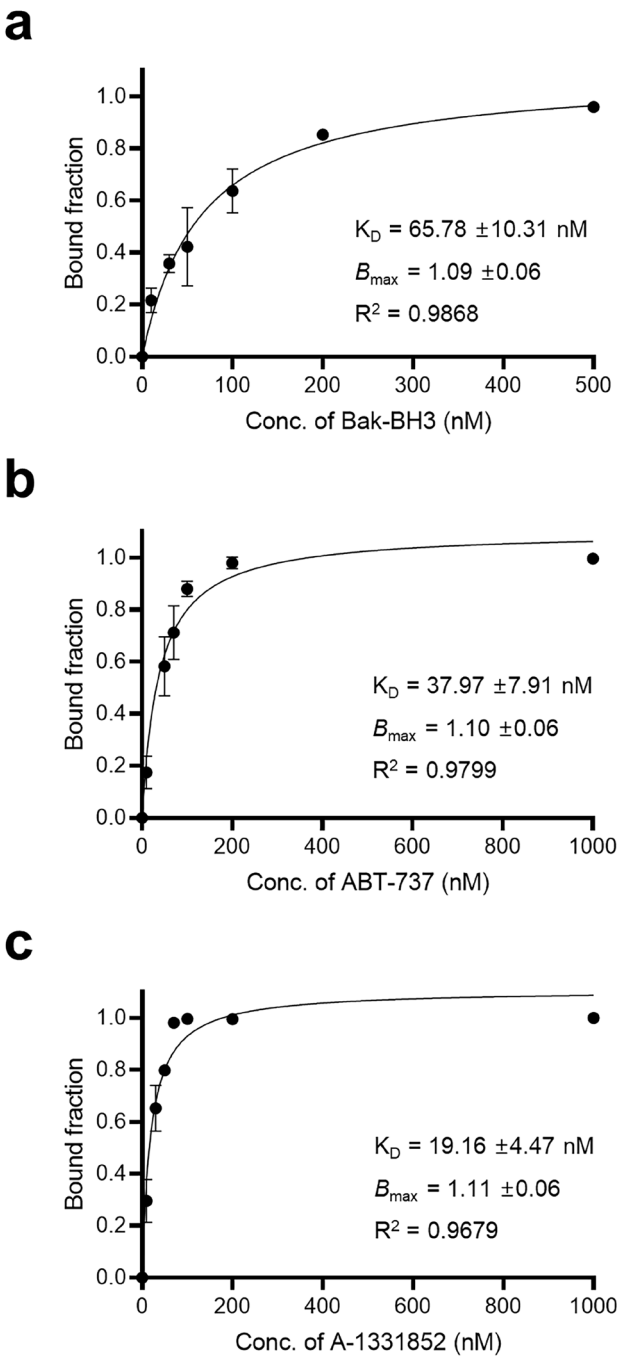


**Supplementary Fig. 17: Current noise ($I_N$) analysis-based determination of Bcl-xL binding affinity for Bak-BH3 peptide, ABT-737, and A-1331852 using YaxAB nanopores. a-c.** Hill diagrams (bound fraction vs. the concentration of ligand) of the Bcl-xL/Bak-BH3 complex (**a**), the Bcl-xL/ABT-737 complex (**b**), and the Bcl-xL/A-1331852 complex (**c**). Data are presented as mean ± SEM, n = 3 independent replicates. Source data are provided as a Source Data file. All measurements were performed by applying 100 mV to the *cis* chamber in 1 M KCl, 10 mM Tris-HCl (pH 7.5), and 1 mM EDTA, with sampling rate of 100 kHz using a 100 Hz Bessel filter. All analytes including Bcl-xL were added to the *cis* chamber.

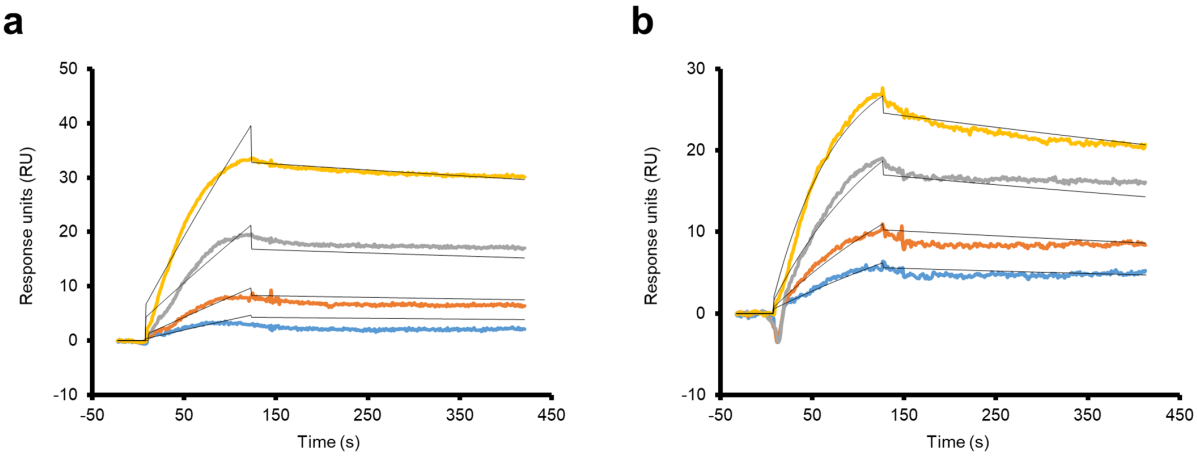


**Supplementary Fig. 18. SPR analysis for interaction between Bcl-xL and small-molecule drugs.** SPR sensorgrams are shown for binding of Bcl-xL with ABT-737 (**a**) and A-1331852 (**b**). The concentrations of small-molecule drugs used are 300 (yellow), 150 (gray), 75 (orange), and 37.5 nM (blue).

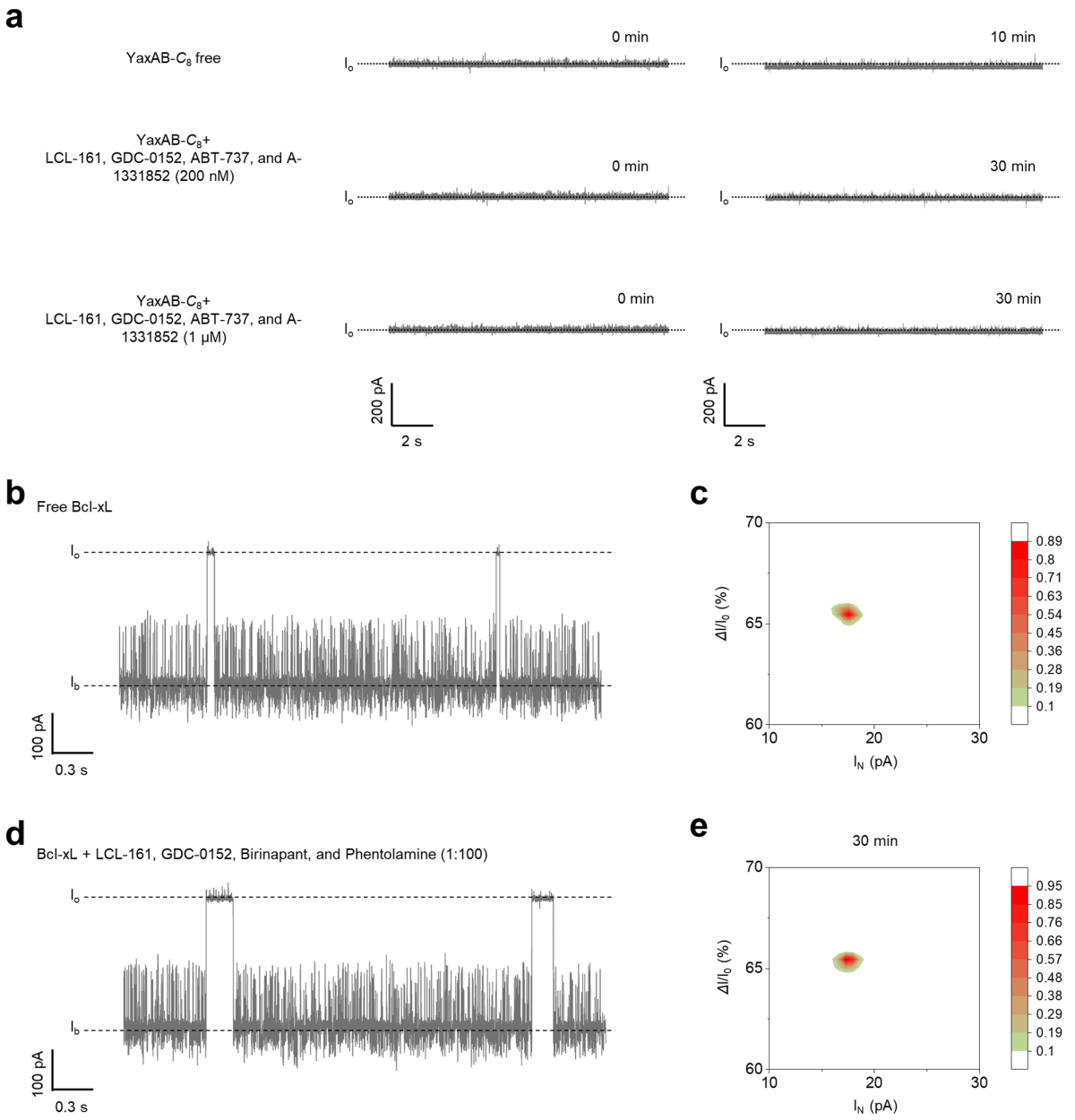


**Supplementary Fig. 19. YaxAB nanopore measurements with non-specific small-molecule ligands. a.** Representative current traces of free YaxAB-$C_8$ and YaxAB-$C_8$ with small-molecule non-binders (LCL-161, GDC-0152, ABT-737, and A-1331852) at 200 nM and 1 µM. **b-e.** Representative multi-level current blockades (**b, d**) and 2D $\Delta I/I_o$-versus-$I_N$ density contour plot of free Bcl-xL and Bcl-xL with small-molecule non-binders (LCL-161, GDC-0152, Birinapant, and Phentolamine) at a molar ratio of 1:100 (**c, e**).

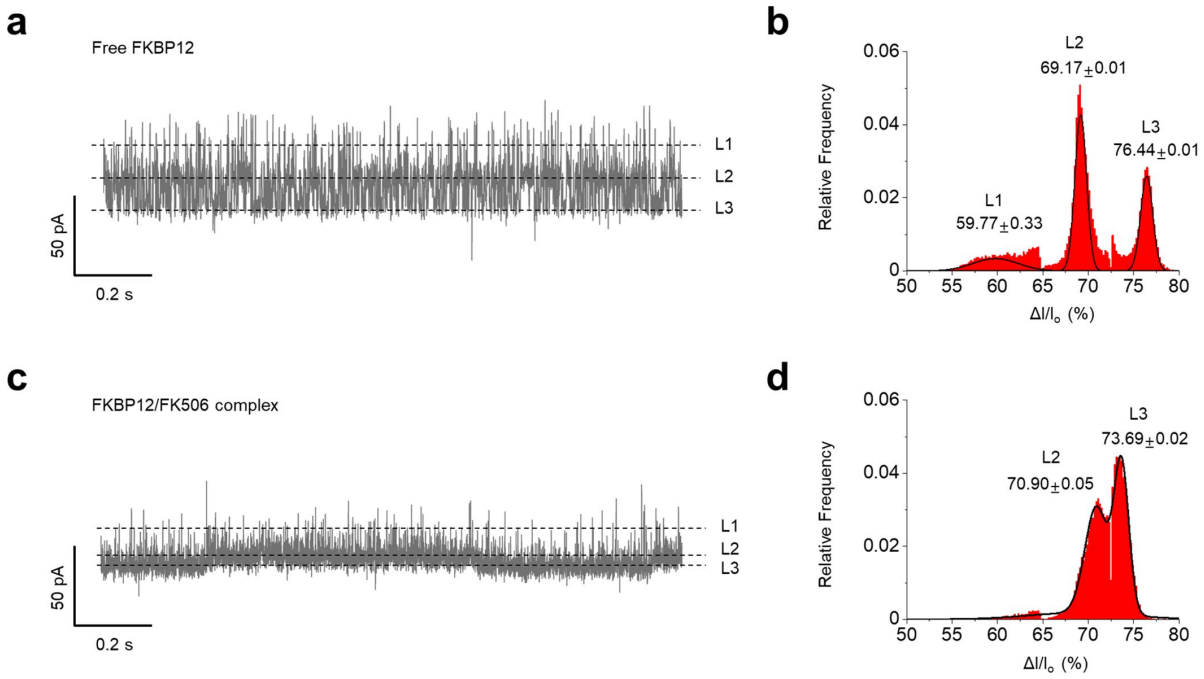


**Supplementary Fig. 20: Detection of FKBP12/FK506 interaction using YaxAB nanopores.** **a-b.** Multi-level current blockades (**a**), and histogram of $\Delta I/I_o$ of free FKBP12 (**b**). **c-d.** Multi-level current blockades (**c**), and histogram of $\Delta I/I_o$ of FKBP12/FK506 complex (**d**).

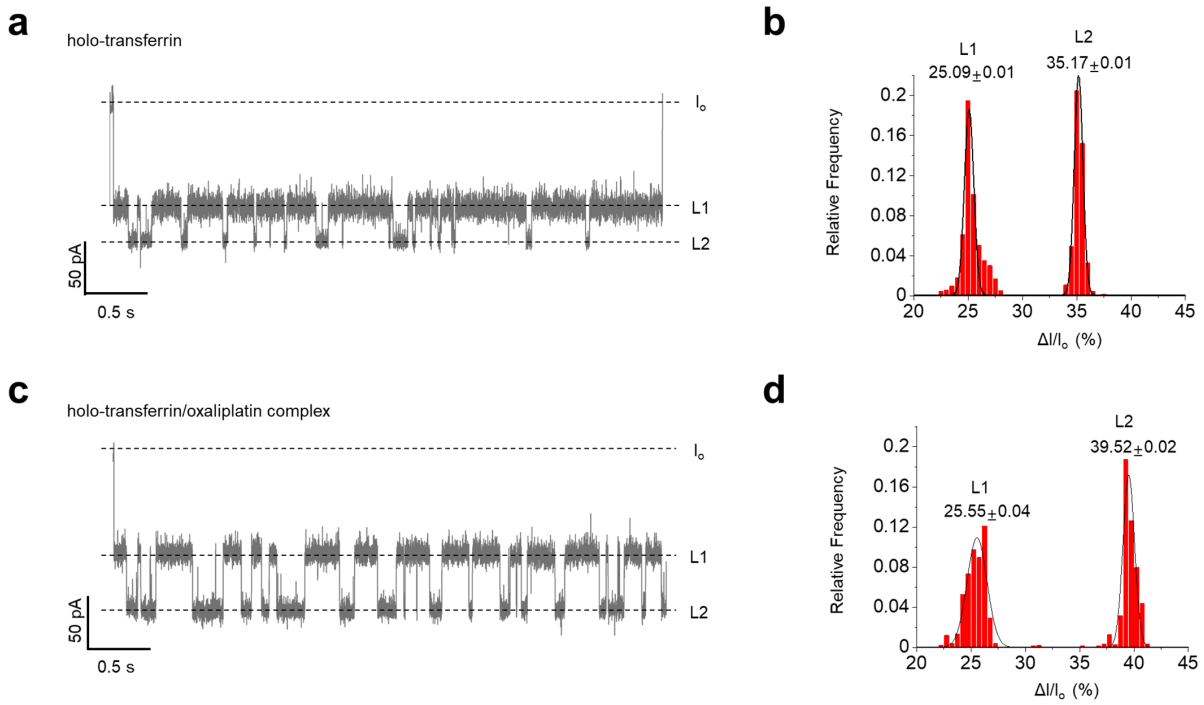


**Supplementary Fig. 21: Detection of holo-transferrin/oxaliplatin interaction using YaxAB nanopores. a-b.** Representative current traces showing multi-level current blockades (L1 and L2) (**a**), and histogram of $\Delta I/I_o$ of free holo-transferrin (**b**). **c-d.** Representative current traces showing multi-level current blockades (L1–L2) (**c**), and histogram of $\Delta I/I_o$ of the holo-transferrin/oxaliplatin complex (**d**).

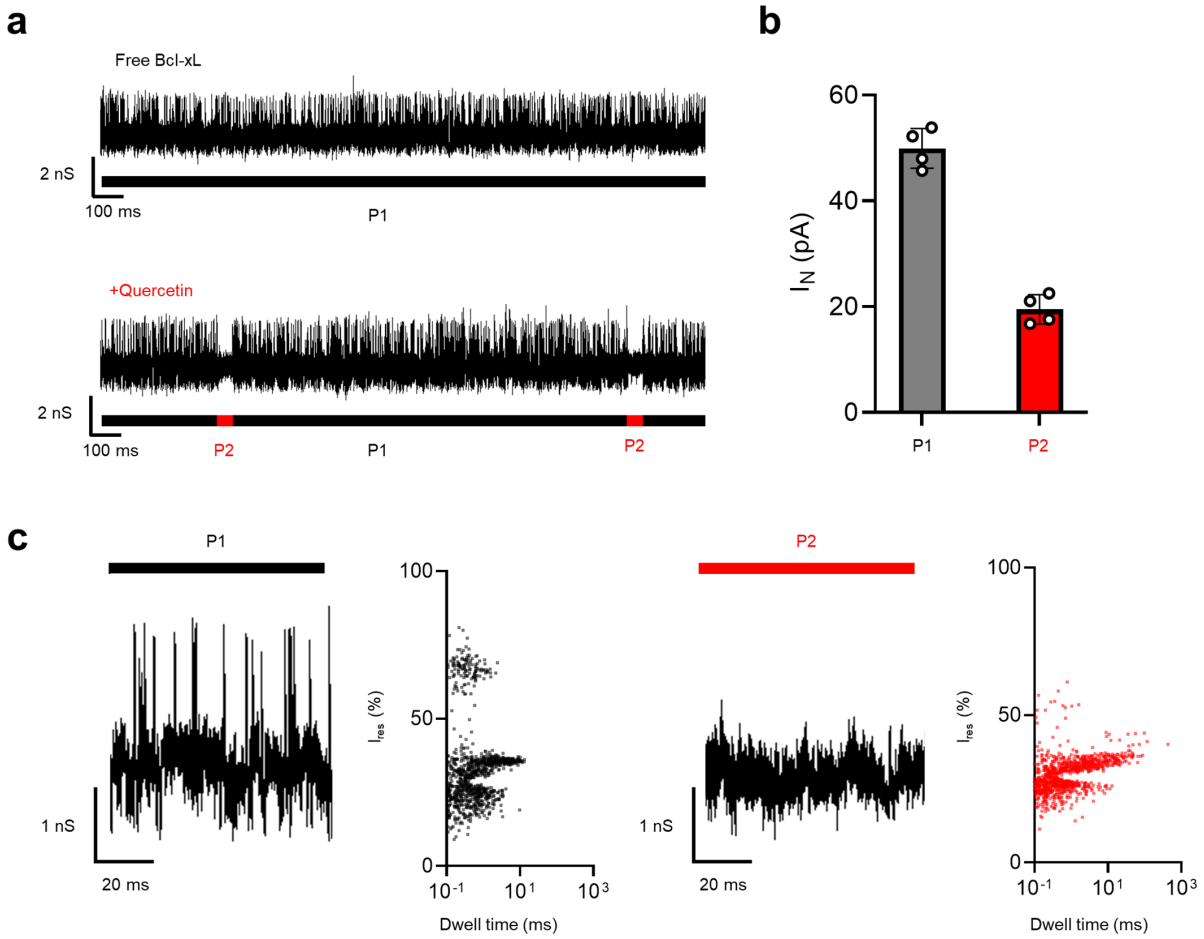


**Supplementary Fig. 22: Current blockade and noise analyses of Bcl-xL/Quercetin interactions using YaxAB nanopores. a.** Representative current traces for free Bcl-xL and the addition of Quercetin. Current signal pattern P1 (black) is temporally transformed to P2 in the presence of Quercetin (red). **b.** Current noise ($I_N$) values of P1 and P2. Data are presented as mean ± SD, n=4 independent replicates for Bcl-xL in the presence of Quercetin. The mean value of $I_N$: P1, 49.17 ± 4.21 pA; P2, 18.95 ± 3.12 pA. Source data are provided as a Source Data file. **c.** Representative zoom-in current traces and corresponding scatter plot ($I_{res}$ vs. dwell time) of Bcl-xL (P1) and the addition of Quercetin (P2). All current traces were recorded at +100 mV in 1 M KCl, 10 mM Tris-HCl, 1 mM EDTA, pH 7.5, with 1 µM Bcl-xL in the presence of Quercetin (at 1:20 molar ratio).

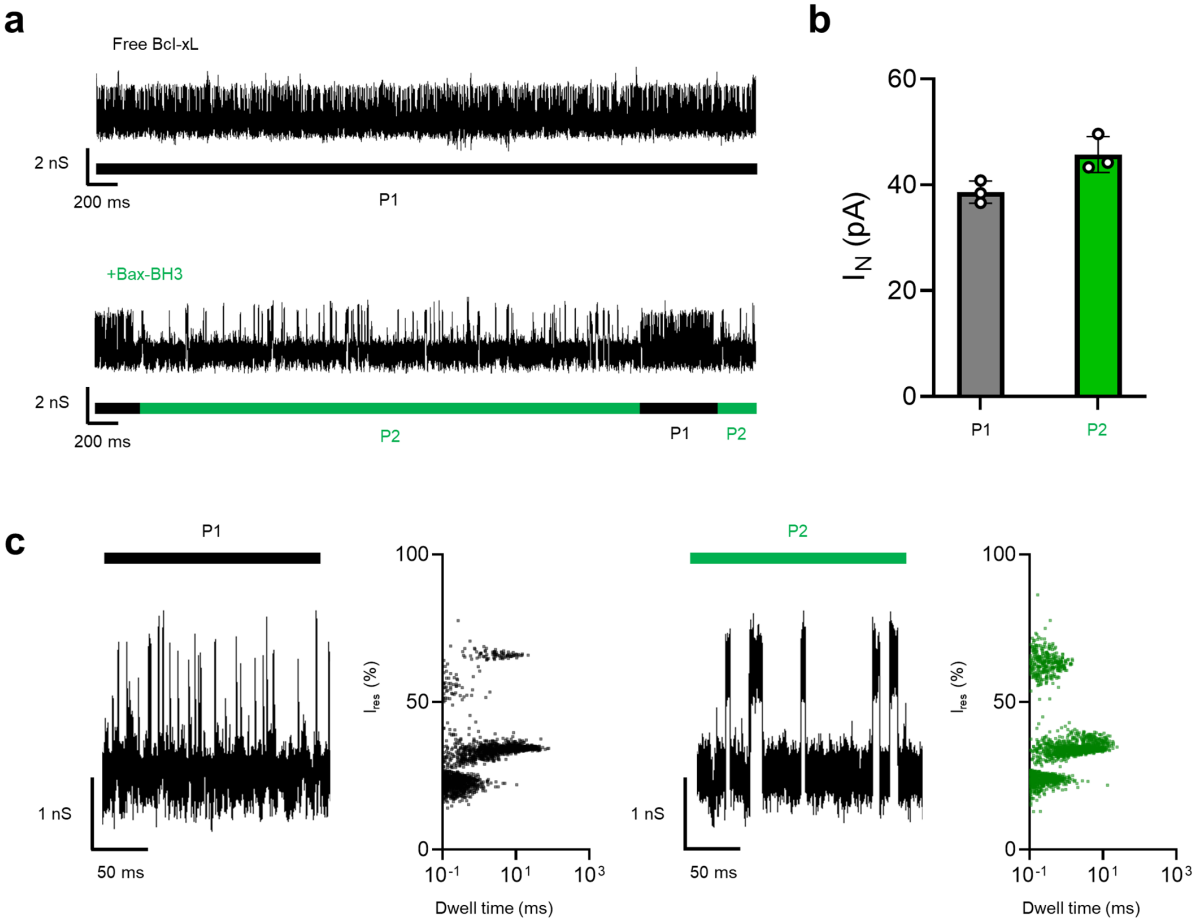


**Supplementary Fig. 23: Current blockade and noise analyses of Bcl-xL/Bax-BH3 interactions using YaxAB nanopores. a.** Representative current traces for free Bcl-xL and the addition of Bax-BH3 peptide. Current signal pattern P1 (black) is temporally transformed to P2 in the presence of Bax-BH3 peptide (green). **b.** Current noise ($I_N$) values of P1 and P2. Data are presented as mean ± SD, n = 3 independent replicates for Bcl-xL in the presence of Bax-BH3 peptide. The mean value of $I_N$: P1, 38.62 ± 2.09 pA; P2, 45.72 ± 3.39 pA. Source data are provided as a Source Data file. **c.** Representative current traces and corresponding scatter plot ($I_{res}$ vs. dwell time) of Bcl-xL (P1) and the addition of Bax-BH3 peptide (P2). All current traces were recorded at +100 mV in 1 M KCl, 10 mM Tris-HCl, 1 mM EDTA, pH 7.5, with 1 µM Bcl-xL in the presence of Bax-BH3 peptide (at 1:100 molar ratio).

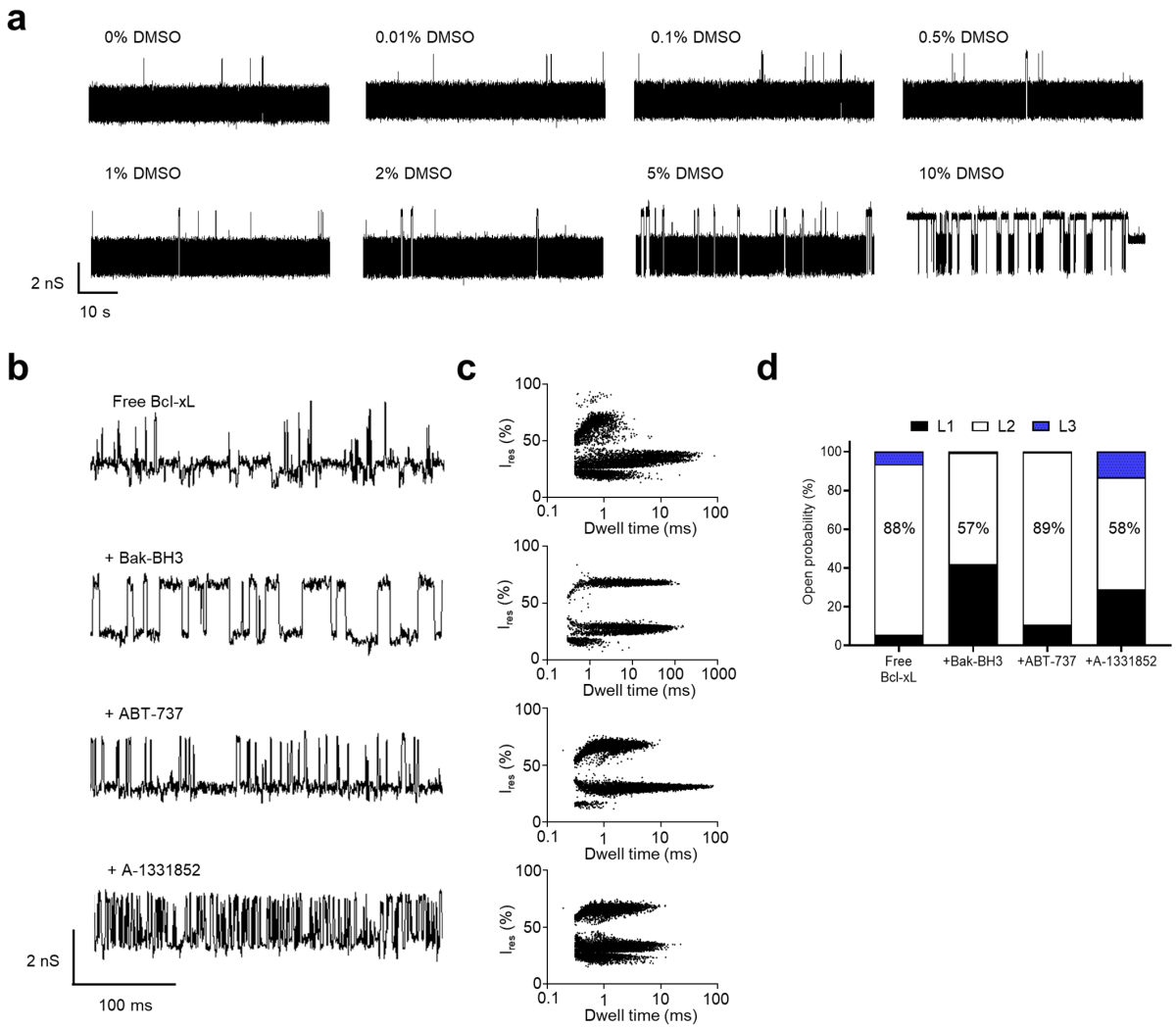


**Supplementary Fig. 24: YaxAB nanopore measurements in the presence of DMSO. a.** Representative current traces of Bcl-xL in the presence of DMSO at various concentrations (0 to 10 %). **b-c.** Representative multi-level current blockades (**b**) and scatter plots ($I_{res}$ vs. dwell time) of Bcl-xL and three complexes, Bcl-xL/Bak-BH3, Bcl-xL/ABT-737, and Bcl-xL/A-1331852 complexes (**c**). **d.** Stacked columns for open probability of L1-L3 levels measured from current blockades of free Bcl-xL and its complexes.

**Supplementary Table 1. Current-voltage (I-V) curves for YaxAB nanopores in symmetric salt conditions at pH 7.5***

| Voltage | YaxAB-$C_{10}$, 1 M KCl | | YaxAB-$C_9$, 1 M KCl | | YaxAB-$C_8$, 1 M KCl | |
|---|---|---|---|---|---|---|
| (mV) | Current (pA) | S.D. | Current (pA) | S.D. | Current (pA) | S.D. |
| -100 | -1165.8 | 23.8 | -898.7 | 21.7 | -639.1 | 9.0 |
| -80 | -928.0 | 28.3 | -707.6 | 11.8 | -501.8 | 5.3 |
| -60 | -687.7 | 18.1 | -526.0 | 8.6 | -369.3 | 3.8 |
| -40 | -453.6 | 16.3 | -347.2 | 5.5 | -241.4 | 1.2 |
| -20 | -223.4 | 11.2 | -172.1 | 2.9 | -117.9 | 0.7 |
| 0 | 0.0 | 0.0 | 0.0 | 0.0 | 0.0 | 0.0 |
| 20 | 227.2 | 4.0 | 167.2 | 3.2 | 113.2 | 1.0 |
| 40 | 450.6 | 7.4 | 328.5 | 5.7 | 220.9 | 2.9 |
| 60 | 668.9 | 10.7 | 484.9 | 9.4 | 321.4 | 3.5 |
| 80 | 881.0 | 14.2 | 633.5 | 11.9 | 416.6 | 5.5 |
| 100 | 1086.5 | 16.9 | 776.0 | 17.2 | 506.1 | 6.4 |

* The buffer contained 1 M KCl, 10 mM Tris-HCl (pH 7.5), and 1 mM EDTA. Each current data represents the average value. Standard deviations are based on data in triplicate. Source data are provided as a Source Data file.

**Supplementary Table 2. Current-voltage (I-V) curves for YaxAB nanopores in asymmetric salt conditions at pH 7.5***

| Voltage | YaxAB-$C_{10}$, 2 M KCl in *trans* | | YaxAB-$C_9$, 2 M KCl in *trans* | | YaxAB-$C_8$, 2 M KCl in *trans* | |
|---|---|---|---|---|---|---|
| (mV) | Current (pA) | S.D. | Current (pA) | S.D. | Current (pA) | S.D. |
| -50 | -646.9 | 44.9 | -487.3 | 13.4 | -349.3 | 34.8 |
| -40 | -522.8 | 34.7 | -395.6 | 7.7 | -282.5 | 28.4 |
| -30 | -402.3 | 22.8 | -306.8 | 3.7 | -221.8 | 21.1 |
| -20 | -282.9 | 14.0 | -218.9 | 2.8 | -161.2 | 15.7 |
| -10 | -170.5 | 11.5 | -133.2 | 2.9 | -105.4 | 9.0 |
| 0 | -53.2 | 9.4 | -49.7 | 3.8 | -51.0 | 4.0 |
| 10 | 61.4 | 9.2 | 31.0 | 4.9 | 1.7 | 2.3 |
| 20 | 172.9 | 11.0 | 108.8 | 6.5 | 51.2 | 6.6 |
| 30 | 280.5 | 13.6 | 184.2 | 8.2 | 99.0 | 10.2 |
| 40 | 388.9 | 11.8 | 255.8 | 9.8 | 144.4 | 15.1 |
| 50 | 488.3 | 18.1 | 326.1 | 11.0 | 187.4 | 18.8 |

* The buffer contained either 2 M or 0.5 M KCl in 10 mM Tris-HCl (pH 7.5) and 1 mM EDTA. Each current data represents the average value. Standard deviations are based on data in triplicate. Source data are provided as a Source Data file.

**Supplementary Table 3. Ion selectivity of YaxAB nanopores**

| Pore type | YaxAB-$C_{10}$ | YaxAB-$C_9$ | YaxAB-$C_8$ |
|---|---|---|---|
| Reversal potential (mV) | 5.48 ± 0.14 | 7.65 ± 0.70 | 11.69 ± 0.14 |
| $P_{K^+}/P_{Cl^-}$ | 1.47 ± 0.01 | 1.72 ± 0.09 | 2.34 ± 0.03 |

Data are presented as mean ± SD, n = 3 independent replicates. Source data are provided as a Source Data file.

**Supplementary Table 4. Molecular properties of Bcl-xL and its complexes**

| Molecule | M.W. (Da) | Excluded volume (Å$^3$) | Dipole moment (D) |
|---|---|---|---|
| Bcl-xL | 20,781.0 | 24,301 | 576.56 |
| Bcl-xL/Bak-BH3* | 22,505.9 | 26,306 | 584.89 |
| Bcl-xL/ABT-737 | 21,594.4 | 24,021 | 430.87 |
| Bcl-xL/A-1331852 | 21,439.8 | 23,756 | 334.18 |

* PDB code: 1BXL